
Mean-field theory of graph neural networks in graph partitioning

Tatsuro Kawamoto, Masashi Tsubaki

Artificial Intelligence Research Center,
National Institute of Advanced Industrial Science and Technology,
2-3-26 Aomi, Koto-ku, Tokyo, Japan
{kawamoto.tatsuro, tsubaki.masashi}@aist.go.jp

Tomoyuki Obuchi

Department of Mathematical and Computing Science, Tokyo Institute of Technology,
2-12-1 Ookayama Meguro-ku Tokyo, Japan
obuchi@c.titech.ac.jp

Abstract

A theoretical performance analysis of the graph neural network (GNN) is presented. For classification tasks, the neural network approach has the advantage in terms of flexibility that it can be employed in a data-driven manner, whereas Bayesian inference requires the assumption of a specific model. A fundamental question is then whether GNN has a high accuracy in addition to this flexibility. Moreover, whether the achieved performance is predominately a result of the backpropagation or the architecture itself is a matter of considerable interest. To gain a better insight into these questions, a mean-field theory of a minimal GNN architecture is developed for the graph partitioning problem. This demonstrates a good agreement with numerical experiments.

1 Introduction

Deep neural networks have been subject to significant attention concerning many tasks in machine learning, and a plethora of models and algorithms have been proposed in recent years. The application of the neural network approach to problems on graphs is no exception and is being actively studied, with applications including social networks and chemical compounds [1, 2]. A neural network model on graphs is termed a graph neural network (GNN) [3]. While excellent performances of GNNs have been reported in the literature, many of these results rely on experimental studies, and seem to be based on the blind belief that the nonlinear nature of GNNs leads to such strong performances. However, when a deep neural network outperforms other methods, the factors that are really essential should be clarified: Is this thanks to the learning of model parameters, e.g., through the backpropagation [4], or rather the architecture of the model itself? Is the choice of the architecture predominantly crucial, or would even a simple choice perform sufficiently well? Moreover, does the GNN generically outperform other methods?

To obtain a better understanding of these questions, not only is empirical knowledge based on benchmark tests required, but also theoretical insights. To this end, we develop a mean-field theory of GNN, focusing on a problem of graph partitioning. The problem concerns a GNN with random model parameters, i.e., an untrained GNN. If the architecture of the GNN itself is essential, then the performance of the untrained GNN should already be effective. On the other hand, if the fine-tuning of the model parameters via learning is crucial, then the result for the untrained GNN is again useful to observe the extent to which the performance is improved.

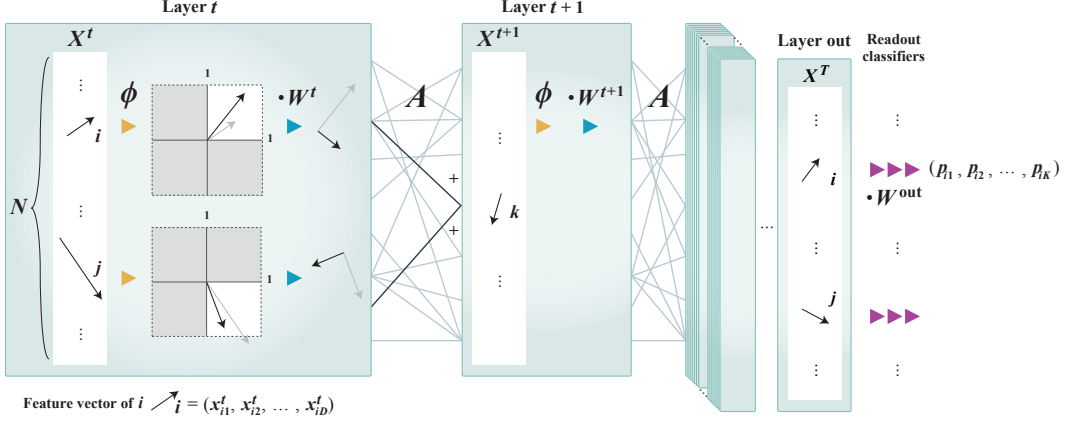


Figure 1: Architecture of the GNN considered in this paper.

Table 1: Comparison of various methods under the framework of Eq. (2).

algorithm	domain	M	$\phi(x)$	$\varphi(x)$	\mathbf{W}^t	\mathbf{b}^t	$\{\mathbf{W}^t, \mathbf{b}^t\}$ update
untrained GNN	V	\mathbf{A}	tanh	$I(x)$	random	omitted	not trained
trained GNN [5]	V	$\mathbf{I} - \mathbf{L}$	ReLU	$I(x)$	trained	omitted	trained via backprop.
Spectral method	V	\mathbf{L}	$I(x)$	$I(x)$	QR	/	updated at each layer
EM + BP	\vec{E}	\mathbf{B}	softmax	$\log(x)$	learned	learned	learned via M-step

For a given graph $G = (V, E)$, where V is the set of vertices and E is the set of (undirected) edges, the graph partitioning problem involves assigning one out of K group labels to each vertex. Throughout this paper, we restrict ourselves to the case of two groups ($K = 2$). The problem setting for graph partitioning is relatively simple compared with other GNN applications. Thus, it is suitable as a baseline for more complicated problems. There are two types of graph partitioning problem: One is to find the best partition for a given graph under a certain objective function. The other is to assume that a graph is generated by a statistical model, and infer the planted (i.e., preassigned) group labels of the generative model. Herein, we consider the latter problem.

Before moving on to the mean-field theory, we first clarify the algorithmic relationship between GNN and other methods of graph partitioning.

2 Graph neural network and its relationship to other methods

The goal of this paper is to examine the graph partitioning performance using a minimal GNN architecture. To this end, we consider a GNN with the following feedforward dynamics. Each vertex is characterized by a D -dimensional feature vector whose elements are $x_{i\mu}$ ($i \in V, \mu \in \{1, \dots, D\}$), and the state matrix $\mathbf{X} = [x_{i\mu}]$ obeys

$$x_{i\mu}^{t+1} = \sum_{j\nu} A_{ij} \phi(x_{j\nu}^t) W_{\nu\mu}^t + b_{i\mu}^t. \quad (1)$$

Throughout this paper, the layers of the GNN are indexed by $t \in \{0, \dots, T\}$. Furthermore, $\phi(x)$ is a nonlinear activation function, $\mathbf{b}^t = [b_{i\mu}^t]$ is a bias term¹, and $\mathbf{W}^t = [W_{\nu\mu}^t]$ is a linear transform that operates on the feature space. To infer the group assignments, a $D \times K$ matrix \mathbf{W}^{out} of the readout classifier is applied at the end of the last layer. Although there is no restriction on ϕ in our mean-field theory, we adopt $\phi = \tanh$ as a specific choice in the experiment below. As there is no detailed attribute on each vertex, the initial state \mathbf{X}^0 is set to be uniformly random, and the adjacency matrix \mathbf{A} is the only input in the present case. For the graphs with vertex attributes, deep neural networks that utilize such information [6–8] are also proposed.

¹The bias term is only included in this section, and will be omitted in later sections.

The set of bias terms $\{\mathbf{b}^t\}$, the linear transforms $\{\mathbf{W}^t\}$ in the intermediate layers, and \mathbf{W}^{out} for the readout classifier are initially set to be random. These are updated through the backpropagation using the training set. In the semi-supervised setting, (real-world) graphs in which only a portion of the vertices are correctly labeled are employed as a training set. On the other hand, in the case of unsupervised learning, graph instances of a statistical model can be employed as the training set.

The GNN architecture described above can be thought of as a special case of the following more general form:

$$x_{i\mu}^{t+1} = \sum_j M_{ij} \varphi \left(\sum_{\nu} \phi(x_{j\nu}^t) W_{\nu\mu}^t \right) + b_{i\mu}^t, \quad (2)$$

where $\varphi(x)$ is another activation function. With different choices for the matrix and activation functions shown in Table 1, various algorithm can be obtained. Equation (1) is recovered by setting $M_{ij} = A_{ij}$ and $\varphi(x) = I(x)$ (where $I(x)$ is the identity function), while [5] employed a Laplacian-like matrix $\mathbf{M} = \mathbf{I} - \mathbf{L} = \mathbf{D}^{-1/2} \mathbf{A} \mathbf{D}^{-1/2}$, where $\mathbf{D}^{-1/2} \equiv \text{diag}(\sqrt{d_1}, \dots, \sqrt{d_N})$ (d_i is the degree of vertex i) and \mathbf{L} is called the normalized Laplacian [9].

The spectral method using the power iteration is obtained in the limit where $\phi(x)$ and $\varphi(x)$ are linear and \mathbf{b}^t is absent.² For the simultaneous power iteration that extracts the leading K eigenvectors, the state matrix \mathbf{X}^0 is set as an $N \times K$ matrix whose column vectors are mutually orthogonal. While the normalized Laplacian \mathbf{L} is commonly adopted for \mathbf{M} , there are several other choices [9–11].³ At each iteration, the orthogonality condition is maintained via QR decomposition [12], i.e., for $\mathbf{Z}^t := \mathbf{M} \mathbf{X}^t$, $\mathbf{X}^{t+1} = \mathbf{Z}^t \mathbf{R}_t^{-1}$, where \mathbf{R}_t^{-1} acts as \mathbf{W}^t . \mathbf{R}_t is a $D \times D$ upper triangular matrix that is obtained by the QR decomposition of \mathbf{Z}^t . Therefore, rather than training \mathbf{W}^t , it is determined at each layer based on the current state.

The belief propagation (BP) algorithm (also called the message passing algorithm) in Bayesian inference also falls under the framework of Eq. (2). While the domain of the state consists of the vertices ($i, j \in V$) for GNNs, this algorithm deals with the directed edges $i \rightarrow j \in \vec{E}$, where \vec{E} is obtained by putting directions to every undirected edge. In this case, the state $x_{\sigma, i \rightarrow j}^t$ represents the logarithm of the marginal probability that vertex i belongs to the group σ with the missing information of vertex j at the t th iteration. With the choice of matrix and activation functions shown in Table 1 (EM+BP), Eq. (2) becomes exactly the update equation of the BP algorithm⁴ [13]. The matrix $\mathbf{M} = \mathbf{B} = [B_{j \rightarrow k, i \rightarrow j}]$ is the so-called non-backtracking matrix [14], and the softmax function represents the normalization of the state $x_{\sigma, i \rightarrow j}^t$.

The BP algorithm requires the model parameters \mathbf{W}^t and \mathbf{b}^t as inputs. For example, when the expectation-maximization (EM) algorithm is considered, the BP algorithm comprises half (the E-step) of the algorithm. The parameter learning of the model is conducted in the other half (the M-step), which can be performed analytically using the current result of the BP algorithm. Here, \mathbf{W}^t and \mathbf{b}^t are the estimates of the so-called density matrix (or affinity matrix) and the external field resulting from messages from non-edges [13], respectively, and are common for every t . Therefore, the differences between the EM algorithm and GNN are summarized as follows. While there is an analogy between the inference procedures, in the EM algorithm the parameter learning of the model is conducted analytically, at the expense of the restrictions of the assumed statistical model. On the other hand, in GNNs the learning is conducted numerically in a data-driven manner [15], for example by backpropagation. While we will shed light on the detailed correspondence in the case of graph partitioning here, the relationship between GNN and BP is also mentioned in [16, 17].

3 Mean-field theory of the detectability limit

3.1 Stochastic block model and its detectability limit

We analyze the performance of an untrained GNN on the stochastic block model (SBM). This is a random graph model with a planted group structure, and is commonly employed as the generative

²Alternatively, it can be regarded that $\text{diag}(b_{i1}^t, \dots, b_{iD}^t)$ is added to \mathbf{W}^t when \mathbf{b}^t has common rows.

³A matrix $\text{const} \cdot \mathbf{I}$ is sometimes added in order to shift the eigenvalues.

⁴Precisely speaking, this is the BP algorithm in which the stochastic block model (SBM) is assumed as the generative model. The SBM is explained below.

model of an inference-based graph clustering algorithm [13, 18–20]. The SBM is defined as follows. We let $|V| = N$, and each of the vertices has a preassigned group label $\sigma \in \{1, \dots, K\}$, i.e., $V = \cup_{\sigma} V_{\sigma}$. We define V_{σ} as the set of vertices in a group σ , $\gamma_{\sigma} \equiv |V_{\sigma}|/N$, and σ_i represents the planted group assignment of vertex i . For each pair of vertices $i \in V_{\sigma}$ and $j \in V_{\sigma'}$, an edge is generated with probability $\rho_{\sigma\sigma'}$, which is an element of the density matrix. Throughout this paper, we assume that $\rho_{\sigma\sigma'} = O(N^{-1})$, so that the resulting graph has a constant average degree, or in other words the graph is sparse. We denote the average degree by c . Therefore, the adjacency matrix $\mathbf{A} = [A_{ij}]$ of the SBM is generated with probability

$$p(\mathbf{A}) = \prod_{i < j} \rho_{\sigma_i \sigma_j}^{A_{ij}} \left(1 - \rho_{\sigma_i \sigma_j}^{A_{ij}}\right)^{1 - A_{ij}}. \quad (3)$$

When $\rho_{\sigma\sigma'}$ is the same for all pairs of σ and σ' , the SBM is nothing but the Erdős-Rényi random graph. Clearly, in this case no algorithm can infer the planted group assignments better than random chance. Interestingly, even when $\rho_{\sigma\sigma'}$ is not constant there exists a limit for the strength of the group structure, below which the planted group assignments cannot be inferred better than chance. This is called the detectability limit. Consider the SBM consisting of two equally-sized groups that is parametrized as $\rho_{\sigma\sigma'} = \rho_{\text{in}}$ for $\sigma = \sigma'$ and $\rho_{\sigma\sigma'} = \rho_{\text{out}}$ for $\sigma \neq \sigma'$, which is often referred to as the symmetric SBM. In this case, it is rigorously known [21–23] that detection is impossible by any algorithm for the SBM with a group structure weaker than

$$\epsilon = (\sqrt{c} - 1)/(\sqrt{c} + 1), \quad (4)$$

where $\epsilon \equiv \rho_{\text{out}}/\rho_{\text{in}}$. However, it is important to note that this is the information-theoretic limit, and the achievable limit for a specific algorithm may not coincide with Eq. (4). For this reason, we investigate the *algorithmic detectability limit* of the GNN here.

3.2 Dynamical mean-field theory

In an untrained GNN, each element of the matrix \mathbf{W}^t is randomly determined according to the Gaussian distribution at each t , i.e., $W_{\nu\mu}^t \sim \mathcal{N}(0, 1/D)$. We assume that the feature dimension D is sufficiently large, but $D/N \ll 1$. Let us consider a state $\mathbf{x}_{\sigma\mu}^t$ that represents the average state within a group, i.e., $\mathbf{x}_{\sigma\mu}^t \equiv (\gamma_{\sigma} N)^{-1} \sum_{i \in V_{\sigma}} x_{i\mu}^t$. The probability distribution that $\mathbf{x}^t = [\mathbf{x}_{\sigma\mu}^t]$ is expressed as

$$P(\mathbf{x}^{t+1}) = \left\langle \prod_{\sigma\mu} \delta \left(\mathbf{x}_{\sigma\mu}^{t+1} - \frac{1}{\gamma_{\sigma} N} \sum_{i \in V_{\sigma}} \sum_{j\nu} A_{ij} \phi(x_{j\nu}^t) W_{\nu\mu}^t \right) \right\rangle_{\mathbf{A}, \mathbf{W}^t, \mathbf{X}^t}, \quad (5)$$

where $\langle \dots \rangle_{\mathbf{A}, \mathbf{W}^t, \mathbf{X}^t}$ denotes the average over the graph \mathbf{A} , the random linear transform \mathbf{W}^t , and the state \mathbf{X}^t of the previous layer. Using the Fourier representation, the normalization condition of Eq. (5) is expressed as

$$1 = \int \mathcal{D}\hat{\mathbf{x}}^{t+1} \mathcal{D}\mathbf{x}^{t+1} e^{-\mathcal{L}_0} \langle e^{\mathcal{L}_1} \rangle_{\mathbf{A}, \mathbf{W}^t, \mathbf{X}^t}, \quad \left\{ \begin{array}{l} \mathcal{L}_0 = \sum_{\sigma\mu} \gamma_{\sigma} \hat{x}_{\sigma\mu}^{t+1} x_{\sigma\mu}^{t+1} \\ \mathcal{L}_1 = \frac{1}{N} \sum_{\mu\nu} \sum_{ij} A_{ij} W_{\nu\mu}^t \hat{x}_{\sigma_i\mu}^{t+1} \phi(x_{j\nu}^t) \end{array} \right\}, \quad (6)$$

where $\hat{x}_{\sigma\mu}^{t+1}$ is an auxiliary variable that is conjugate to $x_{\sigma\mu}^{t+1}$, and $\mathcal{D}\hat{\mathbf{x}}^{t+1} \mathcal{D}\mathbf{x}^{t+1} \equiv \prod_{\sigma\mu} (\gamma_{\sigma} d\hat{x}_{\sigma\mu}^{t+1} dx_{\sigma\mu}^{t+1} / 2\pi i)$.

After taking the average of the symmetric SBM over \mathbf{A} as well as the average over \mathbf{W}^t in the stationary limit with respect to t , the following self-consistent equation is obtained with respect to the covariance matrix $\mathbf{C} = [C_{\sigma\sigma'}]$ of $\mathbf{x} = \mathbf{x}^t$:

$$C_{\sigma\sigma'} = \frac{1}{\gamma_{\sigma} \gamma_{\sigma'}} \sum_{\bar{\sigma}\bar{\sigma}'} B_{\sigma\bar{\sigma}} B_{\sigma'\bar{\sigma}'} \int \frac{d\mathbf{x} e^{-\frac{1}{2} \mathbf{x}^{\top} \mathbf{C}^{-1} \mathbf{x}}}{(2\pi)^{\frac{N}{2}} \sqrt{\det \mathbf{C}}} \phi(x_{\bar{\sigma}}) \phi(x_{\bar{\sigma}'}), \quad (7)$$

where $B_{\sigma\sigma'} \equiv N \gamma_{\sigma} \rho_{\sigma\sigma'} \gamma_{\sigma'}$. The detailed derivation can be found in the supplemental material. The reader may notice that the above expression resembles the recursive equations in [24, 25]. However, it should be noted that Eq. (7) is not obtained as an exact closed equation. The derivation relies mainly on the assumption that the macroscopic random variable \mathbf{x}^t dominates the behavior of the

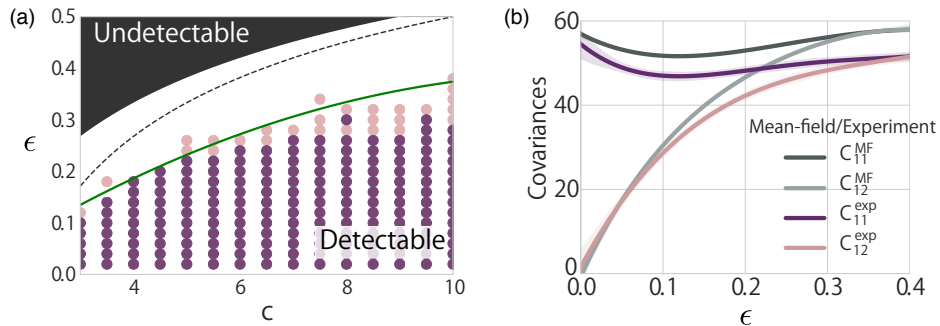


Figure 2: Performance of the untrained GNN evaluated by the behavior of the covariance matrix C . (a) Detectability phase diagram of the SBM. The solid line represents the mean-field estimate by Eq. (7), the dashed line represents the phase boundary of the spectral method (see Section 5 for details), and the dark shaded region represents the region above Eq. (4). The region containing points is that where the covariance gap $C_{11} - C_{12}$ is significantly larger than the gaps in the information-theoretically undetectable region. (b) The curves of the covariances C_{11} and C_{12} of the SBMs with $c = 8$: The mean-field estimates (gray lines that have larger values) and curves obtained by the regression of the experimental data (purple lines with smaller values).

state \mathbf{X}^t . It is numerically confirmed that this assumption appears plausible. This type of analysis is called dynamical mean-field theory (or the Martin-Siggia-Rose formalism) [26–29].

When the correlation within a group $C_{\sigma\sigma}$ is equal to the correlation between groups $C_{\sigma\sigma'}$ ($\sigma \neq \sigma'$), the GNN is deemed to have reached the detectability limit. Beyond the detectability limit, Eq. (7) is no longer a two-component equation, but is reduced to an equation with respect to the variance of one indistinguishable group.

The accuracy of our mean-field estimate is examined in Fig. 2, using the covariance matrix C that we obtained directly from the numerical experiment. In the detectability phase diagram in Fig. 2a, the region that has a covariance gap $C_{11} - C_{12} > \mu_g + 2\sigma_g$ for at least one graph instance among 30 samples is indicated by the dark purple points, and the region with $C_{11} - C_{12} > \mu_g + \sigma_g$ is indicated by the pale purple points, where μ_g and σ_g are the mean and standard deviation, respectively, of the covariance gap in the information-theoretically undetectable region. In Fig. 2b, the elements of the covariance matrix are compared for the SBM with $c = 8$. The consistency of our mean-field estimate is examined for a specific implementation in Section 5.

4 Normalized mutual information error function

The previous section dealt with the feedforward process of an untrained GNN. By employing a classifier such as the k-means method [30], \mathbf{W}^{out} is not required, and the inference of the SBM can be performed without any training procedure. To investigate whether the training significantly improves the performance, the algorithm that updates the matrices $\{\mathbf{W}^t\}$ and \mathbf{W}^{out} must be specified.

The cross-entropy error function is commonly employed to train \mathbf{W}^{out} for a classification task. However, this error function unfortunately cannot be directly applied to the present case. Note that the planted group assignment of SBM is invariant under a global permutation of the group labels. In other words, as long as the set of vertices in the same group share the same label, the label itself can be anything. This is called the identifiability problem [31]. The cross-entropy error function is not invariant under a global label permutation, and thus the classifier cannot be trained unless the degrees of freedom are constrained. A possible brute force approach is to explicitly evaluate all the permutations in the error function [32], although this obviously results in a considerable computational burden unless the number of groups is very small. Note also that semi-supervised clustering does not suffer from the identifiability issue, because the permutation symmetry is explicitly broken.

Here, we instead propose the use of the normalized mutual information (NMI) as an error function for the readout classifier. The NMI is a comparison measure of two group assignments, which naturally eliminates the permutation degrees of freedom. Let $\sigma = \{\sigma_i = \sigma | i \in V_\sigma\}$ be the labels of the planted group assignments, and $\hat{\sigma} = \{\hat{\sigma}_i = \hat{\sigma} | i \in V_{\hat{\sigma}}\}$ be the labels of the estimated group assignments. First, the (unnormalized) mutual information is defined as

$$I(\sigma, \hat{\sigma}) = \sum_{\sigma=1}^K \sum_{\hat{\sigma}=1}^K P_{\sigma\hat{\sigma}} \log \frac{P_{\sigma\hat{\sigma}}}{P_\sigma P_{\hat{\sigma}}}, \quad (8)$$

where the joint probability $P_{\sigma\hat{\sigma}}$ is the fraction of vertices that belong to the group σ in the planted assignment and the group $\hat{\sigma}$ in the estimated assignment. Furthermore, P_σ and $P_{\hat{\sigma}}$ are the marginals of $P_{\sigma\hat{\sigma}}$, and we let $H(\sigma)$ and $H(\hat{\sigma})$ be the corresponding entropies. The NMI is defined by

$$\text{NMI}(\sigma, \hat{\sigma}) \equiv \frac{2I(\sigma, \hat{\sigma})}{H(\sigma) + H(\hat{\sigma})}. \quad (9)$$

We adopt this measure as the error function for the readout classifier. For the resulting state $x_{i\mu}^T$, the estimated assignment probability $p_{i\sigma}$ that vertex i belongs to the group σ is defined as $p_{i\sigma} \equiv \text{softmax}(a_{i\sigma})$, where $a_{i\sigma} = \sum_{\mu} x_{i\mu} W_{\mu\sigma}^{\text{out}}$. Each element of the NMI is then obtained as

$$\begin{aligned} P_{\sigma\hat{\sigma}} &= \frac{1}{N} \sum_{i=1}^N P(i \in V_\sigma, i \in V_{\hat{\sigma}}) = \frac{1}{N} \sum_{i \in V_\sigma} p_{i\hat{\sigma}}, \\ P_\sigma &= \sum_{\hat{\sigma}} P_{\sigma\hat{\sigma}} = \gamma_\sigma, \quad P_{\hat{\sigma}} = \sum_{\sigma} P_{\sigma\hat{\sigma}} = \frac{1}{N} \sum_{i=1}^N p_{i\hat{\sigma}}. \end{aligned} \quad (10)$$

In summary,

$$\text{NMI}([P_{\sigma\hat{\sigma}}]) = 2 \left(1 - \frac{\sum_{\sigma\hat{\sigma}} P_{\sigma\hat{\sigma}} \log P_{\sigma\hat{\sigma}}}{\sum_{\sigma} \gamma_\sigma \log \gamma_\sigma + \sum_{\sigma\hat{\sigma}} P_{\sigma\hat{\sigma}} \log \sum_{\sigma} P_{\sigma\hat{\sigma}}} \right). \quad (11)$$

This measure is permutation invariant, because the NMI counts the label co-occurrence patterns for each vertex in σ and $\hat{\sigma}$.

5 Experiments

First, the consistency between our mean-field theory and a specific implementation of an untrained GNN is examined. The performance of the untrained GNN is evaluated by drawing phase diagrams. For the SBMs with various values for the average degree c and the strength of group structure ϵ , the overlap, i.e., the fraction of vertices that coincide with their planted labels, is calculated. Afterward, it is investigated whether a significant improvement is achieved through the parameter learning of the model. Note that because even a completely random clustering can correctly infer half of the labels on average, the minimum of the overlap is 0.5.⁵ As mentioned above, we adopt $\phi = \tanh$ as the specific choice of activation function.

5.1 Untrained GNN with the k-means classifier

We evaluate the performance of the untrained GNN in which the resulting state \mathbf{X} is read out using the k-means (more precisely k-means++ [30]) classifier. In this case, no parameter learning takes place. We set the dimension of the feature space to $D = 100$ and the number of layers to $T = 100$, and each result represents the average over 30 samples.

Figure 3a presents the corresponding phase diagram. The overlap is indicated by colors, and the solid line represents the detectability limit estimated by Eq. (7). The dashed line represents the mean-field estimate of the detectability limit of the spectral method⁶ [33, 34], and the shaded area represents

⁵For this reason, the overlap is sometimes standardized such that the minimum equals zero.

⁶Again, there are several choices for the matrix to be adopted in the spectral method. However, the Laplacians and modularity matrix, for example, have the same detectability limit when the graph is regular or the average degree is sufficiently large.

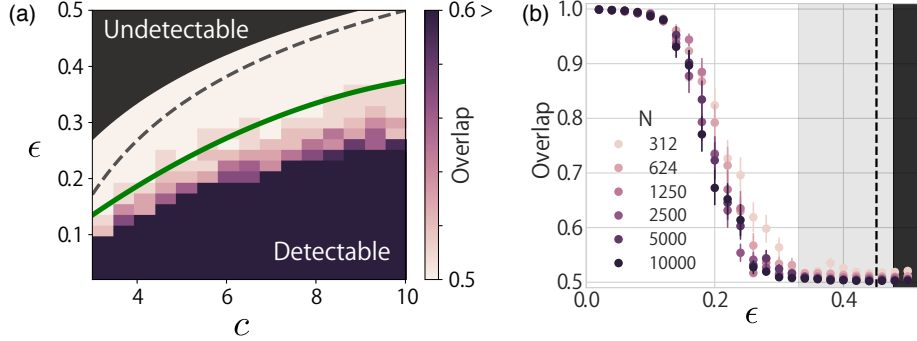


Figure 3: Performance of the untrained GNN using the k-means classifier. (a) The same detectability phase diagram as in Fig. 2. The heatmap represents the overlap obtained using the untrained GNN. (b) The overlaps of the SBM with $c = 8$: The light shaded area represents the region above the estimate using Eq. (7), the dashed line represents the detectability limit of the spectral method, and the dark shaded region represents the information-theoretically undetectable region.

the region above which the inference is information-theoretically impossible. It is known that the detectability limit of the BP algorithm [13] coincides with this information-theoretic limit so long as the model parameters are correctly learned. For the present model, it is also known that the EM algorithm can indeed learn these parameters [35]. Note that it is natural that a Bayesian method will outperform others as long as a consistent model is used, whereas it may perform poorly if the assumed model is not consistent.

It can be observed that our mean-field estimate exhibits a good agreement with the numerical experiment. For a closer view, the overlaps of multiple graph sizes with $c = 8$ are presented in Fig. 3b. For $c = 8$, the estimate is $\epsilon^* \approx 0.33$, and this appears to coincide with the point at which the overlap is almost 0.5. It should be noted that the performance can vary depending on the implementation details. For example, while the k-means method is performed to \mathbf{X}^T in the present experiment, it can instead be performed to $\phi(\mathbf{X}^T)$. An experiment concerning such a case is presented in the supplemental material.

5.2 GNN with backpropagation and a trained classifier

Now, we consider a trained GNN, and compare its performance with the untrained one. A set of SBM instances is provided as the training set. This consists of 1,000 SBM instances with $N = 5,000$, where an average degree $c \in \{3, 4, \dots, 10\}$ and strength of the group structure $\epsilon \in \{0.05, 0.1, \dots, 0.5\}$ are adopted. For the validation (development) set, 100 graph instances of the same SBMs are provided. Finally, the SBMs with various values of ϵ and the average degree $c = 8$ are provided as the test set.

We evaluated the performance of a GNN trained by backpropagation. We implemented the GNN using Chainer (version 3.2.0) [36]. As in the previous section, the dimension of the feature space is set to $D = 100$, and various numbers of layers are examined. For the error function of the readout classifier, we adopted the NMI error function described in Section 4. The model parameters are optimized using the default setting of the Adam optimizer [37] in Chainer. Although we examined various optimization procedures for fine-tuning, the improvement was hardly observable.

We also employ residual networks (ResNets) [38] and batch normalization (BN) [39]. These are also adopted in [32]. The ResNet imposes skip (or shortcut) connections on a deep network, i.e., $x_{i\mu}^{t+1} = \sum_{j\nu} A_{ij} \phi(x_{j\nu}^t) W_{\nu\mu}^t + x_{i\mu}^{t-s}$, where s is the number of layers skipped, and is set as $s = 5$. The BN layer, which standardizes the distribution of the state \mathbf{X}^t , is placed at each intermediate layer t . Finally, we note that the parameters of deep GNNs (e.g., $T > 25$) cannot be learned correctly without using the ResNet and BN techniques.

The results using the GNN trained as above are illustrated in Fig. 4. First, it can be observed from Fig. 4a that a deep structure is important for a better accuracy. For sufficiently deep networks, the

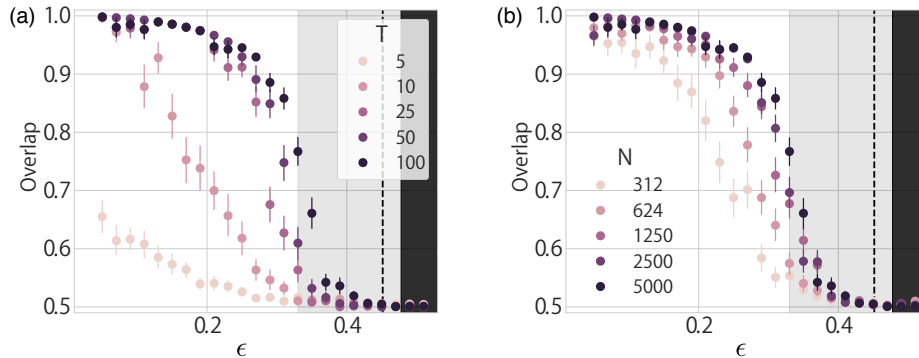


Figure 4: Overlaps of the GNN with trained model parameters. (a) The overlaps of the GNN with various number of layers T on the SBM with $c = 8$ and $N = 5,000$. (b) The graph size dependence of the overlap of the GNN with $T = 100$ on the SBM with $c = 8$. In both cases, the shaded regions and dashed line are plotted in the same manner as in Fig. 3b.

overlaps obtained by the trained GNN are clearly better than those of the untrained counterpart (see Fig. 3b). On the other hand, the region of ϵ where the overlap suddenly deteriorates still coincides with our mean-field estimate for the untrained GNN. This implies that in the limit $N \rightarrow \infty$, the detectability limit is not significantly improved by training. To demonstrate the finite-size effect in the result of Fig. 4a, the overlaps of various graph sizes are plotted in Fig. 4b. The variation of overlaps becomes steeper around $\epsilon^* \approx 0.33$ as the graph size is increased, implying the presence of detectability phase transition around the value of ϵ predicted by our mean-field estimate.

The untrained and trained GNNs exhibit a clear difference in overlap when \mathbf{X}^T is employed as the readout classifier. However, it should be noted that the untrained GNN where $\phi(\mathbf{X}^T)$ is adopted as the readout classifier exhibits a performance close to that of the trained GNN. The reader should also bear in mind that the computational cost required for training is not negligible.

6 Discussion

In a minimal GNN model, the adjacency matrix \mathbf{A} is employed for the connections between intermediate layers. In fact, there have been many attempts [5, 32, 40, 41] to adopt a more complex architecture rather than \mathbf{A} . Furthermore, other types of applications of deep neural networks to graph partitioning or related problems have been described [6, 7, 42]. The number of GNN varieties can be arbitrarily extended by modifying the architecture and learning algorithm. Again, it is important to clarify which elements are essential for the performance.

The present study offers a baseline answer to this question. Our mean-field theory and numerical experiment using the k-means readout classifier clarify that an untrained GNN with a simple architecture already performs well. It is worth noting that our mean-field theory yields an accurate estimate of the detectability limit in a compact form. The learning of the model parameters by backpropagation does contribute to an improved accuracy, although this appears to be quantitatively insignificant. Importantly, the detectability limit appears to remain (almost) the same.

The minimal GNN that we considered in this paper is not the state of the art for the inference of the symmetric SBM. However, as described in Section 2, an advantage of the GNN is its flexibility, in that the model can be learned in a data-driven manner. For a more complicated example, such as the graphs of chemical compounds in which each vertex has attributes, the GNN is expected to generically outperform other approaches. In such a case, the performance may be significantly improved thanks to backpropagation. This would constitute an interesting direction for future work. In addition, the adequacy of the NMI error function that we introduced for the readout classifier should be examined in detail.

Acknowledgments

The authors are grateful to Ryo Karakida for helpful comments. This work was supported by the New Energy and Industrial Technology Development Organization (NEDO) (T.K. and M. T.) and JSPS KAKENHI No. 18K11463 (T. O.).

References

- [1] Aditya Grover and Jure Leskovec. node2vec: Scalable feature learning for networks. In *International Conference on Knowledge Discovery and Data Mining*, 2016.
- [2] David K. Duvenaud, Dougal Maclaurin, Jorge Iparraguirre, Rafael Bombarell, Timothy Hirzel, Alan Aspuru-Guzik, and Ryan P. Adams. Convolutional networks on graphs for learning molecular fingerprints. In *Advances in Neural Information Processing Systems*, 2015.
- [3] Franco Scarselli, Marco Gori, Ah Chung Tsoi, Markus Hagenbuchner, and Gabriele Monfardini. The graph neural network model. *Trans. Neur. Netw.*, 20(1):61–80, January 2009.
- [4] David E Rumelhart, Geoffrey E Hinton, and Ronald J Williams. Learning representations by back-propagating errors. *nature*, 323(6088):533, 1986.
- [5] Thomas N Kipf and Max Welling. Semi-supervised classification with graph convolutional networks. *arXiv preprint arXiv:1609.02907*, 2016.
- [6] Mathias Niepert, Mohamed Ahmed, and Konstantin Kutzkov. Learning convolutional neural networks for graphs. In *International conference on machine learning*, pages 2014–2023, 2016.
- [7] Will Hamilton, Zhitao Ying, and Jure Leskovec. Inductive representation learning on large graphs. In I. Guyon, U. V. Luxburg, S. Bengio, H. Wallach, R. Fergus, S. Vishwanathan, and R. Garnett, editors, *Advances in Neural Information Processing Systems 30*, pages 1024–1034. Curran Associates, Inc., 2017.
- [8] Tao Lei, Wengong Jin, Regina Barzilay, and Tommi Jaakkola. Deriving neural architectures from sequence and graph kernels. In Doina Precup and Yee Whye Teh, editors, *Proceedings of the 34th International Conference on Machine Learning*, volume 70 of *Proceedings of Machine Learning Research*, pages 2024–2033, International Convention Centre, Sydney, Australia, 06–11 Aug 2017. PMLR.
- [9] Ulrike Luxburg. A tutorial on spectral clustering. *Statistics and Computing*, 17(4):395–416, August 2007.
- [10] M. E. J. Newman. Finding community structure in networks using the eigenvectors of matrices. *Phys. Rev. E*, 74:036104, 2006.
- [11] Karl Rohe, Sourav Chatterjee, and Bin Yu. Spectral clustering and the high-dimensional stochastic blockmodel. *The Annals of Statistics*, 39(4):1878–1915, 2011.
- [12] Gene H Golub and Charles F Van Loan. *Matrix computations*, volume 3. JHU Press, 2012.
- [13] Aurelien Decelle, Florent Krzakala, Cristopher Moore, and Lenka Zdeborová. Asymptotic analysis of the stochastic block model for modular networks and its algorithmic applications. *Phys. Rev. E*, 84:066106, 2011.
- [14] Florent Krzakala, Cristopher Moore, Elchanan Mossel, Joe Neeman, Allan Sly, Lenka Zdeborová, and Pan Zhang. Spectral redemption in clustering sparse networks. *Proc. Natl. Acad. Sci. U.S.A.*, 110(52):20935–40, December 2013.
- [15] Jiaxuan You, Rex Ying, Xiang Ren, William L Hamilton, and Jure Leskovec. GraphRNN: A deep generative model for graphs. *arXiv preprint arXiv:1802.08773*, 2018.
- [16] Justin Gilmer, Samuel S Schoenholz, Patrick F Riley, Oriol Vinyals, and George E Dahl. Neural message passing for quantum chemistry. *arXiv preprint arXiv:1704.01212*, 2017.

- [17] Michael Schlichtkrull, Thomas N Kipf, Peter Bloem, Rianne van den Berg, Ivan Titov, and Max Welling. Modeling relational data with graph convolutional networks. *arXiv preprint arXiv:1703.06103*, 2017.
- [18] Tiago P. Peixoto. Efficient monte carlo and greedy heuristic for the inference of stochastic block models. *Phys. Rev. E*, 89:012804, Jan 2014.
- [19] Tiago P Peixoto. Bayesian stochastic blockmodeling. *arXiv preprint arXiv:1705.10225*, 2017.
- [20] M. E. J. Newman and Gesine Reinert. Estimating the number of communities in a network. *Phys. Rev. Lett.*, 117:078301, Aug 2016.
- [21] Elchanan Mossel, Joe Neeman, and Allan Sly. Reconstruction and estimation in the planted partition model. *Probability Theory and Related Fields*, 162(3):431–461, Aug 2015.
- [22] Laurent Massoulié. Community detection thresholds and the weak ramanujan property. In *Proceedings of the 46th Annual ACM Symposium on Theory of Computing*, STOC '14, pages 694–703, New York, 2014. ACM.
- [23] Cristopher Moore. The computer science and physics of community detection: landscapes, phase transitions, and hardness. *arXiv preprint arXiv:1702.00467*, 2017.
- [24] Ben Poole, Subhaneil Lahiri, Maithra Raghu, Jascha Sohl-Dickstein, and Surya Ganguli. Exponential expressivity in deep neural networks through transient chaos. In D. D. Lee, M. Sugiyama, U. V. Luxburg, I. Guyon, and R. Garnett, editors, *Advances in Neural Information Processing Systems 29*, pages 3360–3368. Curran Associates, Inc., 2016.
- [25] Samuel S Schoenholz, Justin Gilmer, Surya Ganguli, and Jascha Sohl-Dickstein. Deep information propagation. *arXiv preprint arXiv:1611.01232*, 2016.
- [26] H. Sompolinsky and Annette Zippelius. Relaxational dynamics of the edwards-anderson model and the mean-field theory of spin-glasses. *Phys. Rev. B*, 25:6860–6875, Jun 1982.
- [27] A. Crisanti and H. Sompolinsky. Dynamics of spin systems with randomly asymmetric bonds: Ising spins and glauher dynamics. *Phys. Rev. A*, 37:4865–4874, Jun 1988.
- [28] A Crisanti, HJ Sommers, and H Sompolinsky. Chaos in neural networks: chaotic solutions. *preprint*, 1990.
- [29] Manfred Opper, Burak Çakmak, and Ole Winther. A theory of solving tap equations for ising models with general invariant random matrices. *Journal of Physics A: Mathematical and Theoretical*, 49(11):114002, 2016.
- [30] David Arthur and Sergei Vassilvitskii. K-means++: The advantages of careful seeding. In *Proceedings of the Eighteenth Annual ACM-SIAM Symposium on Discrete Algorithms*, SODA '07, pages 1027–1035, Philadelphia, PA, USA, 2007. Society for Industrial and Applied Mathematics.
- [31] Krzysztof Nowicki and Tom A. B Snijders. Estimation and prediction for stochastic blockstructures. *Journal of the American Statistical Association*, 96(455):1077–1087, 2001.
- [32] Joan Bruna and Xiang Li. Community detection with graph neural networks. *arXiv preprint arXiv:1705.08415*, 2017.
- [33] Tatsuhiro Kawamoto and Yoshiyuki Kabashima. Limitations in the spectral method for graph partitioning: Detectability threshold and localization of eigenvectors. *Phys. Rev. E*, 91:062803, Jun 2015.
- [34] T. Kawamoto and Y. Kabashima. Detectability of the spectral method for sparse graph partitioning. *Eur. Phys. Lett.*, 112(4):40007, 2015.
- [35] Tatsuhiro Kawamoto. Algorithmic detectability threshold of the stochastic block model. *Phys. Rev. E*, 97:032301, Mar 2018.

- [36] Seiya Tokui, Kenta Oono, Shohei Hido, and Justin Clayton. Chainer: a next-generation open source framework for deep learning. In *Proceedings of workshop on machine learning systems (LearningSys) in the twenty-ninth annual conference on neural information processing systems*, 2015.
- [37] Diederik P Kingma and Jimmy Ba. Adam: A method for stochastic optimization. *arXiv preprint arXiv:1412.6980*, 2014.
- [38] Kaiming He, Xiangyu Zhang, Shaoqing Ren, and Jian Sun. Deep residual learning for image recognition. In *Proceedings of the IEEE conference on computer vision and pattern recognition*, 2016.
- [39] Sergey Ioffe and Christian Szegedy. Batch normalization: Accelerating deep network training by reducing internal covariate shift. *arXiv preprint arXiv:1502.03167*, 2015.
- [40] Joan Bruna, Wojciech Zaremba, Arthur Szlam, and Yann LeCun. Spectral networks and locally connected networks on graphs. *arXiv preprint arXiv:1312.6203*, 2013.
- [41] Michaël Defferrard, Xavier Bresson, and Pierre Vandergheynst. Convolutional neural networks on graphs with fast localized spectral filtering. In D. D. Lee, M. Sugiyama, U. V. Luxburg, I. Guyon, and R. Garnett, editors, *Advances in Neural Information Processing Systems 29*, pages 3844–3852. Curran Associates, Inc., 2016.
- [42] Liang Yang, Xiaochun Cao, Dongxiao He, Chuan Wang, Xiao Wang, and Weixiong Zhang. Modularity based community detection with deep learning. In *Proceedings of the Twenty-Fifth International Joint Conference on Artificial Intelligence, IJCAI'16*, pages 2252–2258. AAAI Press, 2016.

A Derivation of the self-consistent equation

In this section, the detailed derivation of the self-consistent equation of the covariance matrix is derived. Here, we recast our starting-point equation:

$$1 = \int \mathcal{D}\hat{\mathbf{x}}^{t+1} \mathcal{D}\mathbf{x}^{t+1} e^{-\mathcal{L}_0} \langle e^{\mathcal{L}_1} \rangle_{A, W^t, X^t}, \quad \begin{cases} \mathcal{L}_0 = \sum_{\sigma\mu} \gamma_{\sigma} \hat{x}_{\sigma\mu}^{t+1} x_{\sigma\mu}^{t+1} \\ \mathcal{L}_1 = \frac{1}{N} \sum_{\mu\nu} \sum_{ij} A_{ij} W_{\nu\mu}^t \hat{x}_{\sigma_i\mu}^{t+1} \phi(x_{j\nu}^t). \end{cases} \quad (12)$$

A.1 Random averages over W^t and A

We first take the average of $\exp(\mathcal{L}_1)$ over W^t . The Gaussian integral with respect to W^t yields

$$\begin{aligned} \langle e^{\mathcal{L}_1} \rangle_{W^t} &= \exp \left(\frac{1}{2DN^2} \sum_{\mu\nu} \sum_{ijkl} A_{ij} \hat{x}_{\sigma_i\mu}^{t+1} \phi(x_{j\nu}^t) A_{kl} \hat{x}_{\sigma_k\mu}^{t+1} \phi(x_{l\nu}^t) \right) \\ &= \exp \left(\frac{1}{2D} \sum_{\sigma_1\sigma_2\sigma_3\sigma_4} \sum_{\mu} \hat{x}_{\sigma_1\mu}^{t+1} \hat{x}_{\sigma_3\mu}^{t+1} \sum_{\nu} \psi_{\sigma_1\sigma_2}^{t,\nu} \psi_{\sigma_3\sigma_4}^{t,\nu} \right) = \exp \left(\frac{D}{2} \sum_{\sigma_1\sigma_3} u_{\sigma_1\sigma_3}^{t+1} v_{\sigma_1\sigma_3}^t \right), \end{aligned} \quad (13)$$

where we introduce the following quantities:

$$\psi_{\sigma\sigma'}^{t,\nu} \equiv \frac{1}{N} \sum_{i \in V_{\sigma}} \sum_{j \in V_{\sigma'}} A_{ij} \phi(x_{j\nu}^t), \quad (14)$$

$$u_{\sigma\sigma'}^{t+1} \equiv \frac{1}{D} \sum_{\mu} \hat{x}_{\sigma\mu}^{t+1} \hat{x}_{\sigma'\mu}^{t+1}, \quad (15)$$

$$v_{\sigma\sigma'}^t \equiv \frac{1}{D} \sum_{\mu} \sum_{\tilde{\sigma}\tilde{\sigma}'} \psi_{\sigma\tilde{\sigma}}^{t,\mu} \psi_{\tilde{\sigma}'\sigma'}^{t,\mu}. \quad (16)$$

Therefore, Eq. (12) can be written as

$$\begin{aligned} 1 &= \int \mathcal{D}\hat{\mathbf{x}}^{t+1} \mathcal{D}\mathbf{x}^{t+1} \left\langle \int \mathcal{D}\hat{\mathbf{u}}^{t+1} \mathcal{D}\mathbf{u}^{t+1} \int \mathcal{D}\hat{\mathbf{v}}^t \mathcal{D}\mathbf{v}^t \int \mathcal{D}\hat{\psi}^t \mathcal{D}\psi^t \right. \\ &\quad \times \left\langle \exp \left[-\mathcal{L}_0 + \frac{D}{2} \sum_{\sigma\sigma'} u_{\sigma\sigma'}^{t+1} v_{\sigma\sigma'}^t - \sum_{\sigma\sigma'} \hat{u}_{\sigma\sigma'}^{t+1} \left(D u_{\sigma\sigma'}^{t+1} - \sum_{\mu} \hat{x}_{\sigma\mu}^{t+1} \hat{x}_{\sigma'\mu}^{t+1} \right) \right. \right. \\ &\quad \left. \left. - \sum_{\sigma\sigma'} \hat{v}_{\sigma\sigma'}^t \left(D v_{\sigma\sigma'}^t - \sum_{\nu} \sum_{\tilde{\sigma}\tilde{\sigma}'} \psi_{\sigma\tilde{\sigma}}^{t,\nu} \psi_{\tilde{\sigma}'\sigma'}^{t,\nu} \right) \right. \right. \\ &\quad \left. \left. - \sum_{\sigma\sigma'} \sum_{\mu} \hat{\psi}_{\sigma\sigma'}^{t,\mu} \left(\psi_{\sigma\sigma'}^{t,\mu} - \frac{1}{N} \sum_{i \in V_{\sigma}} \sum_{j \in V_{\sigma'}} A_{ij} \phi(x_{j\mu}^t) \right) \right] \right\rangle_A \right\rangle_{X^t}. \end{aligned} \quad (17)$$

Note that as we will see below, \mathbf{u}^{t+1} , \mathbf{v}^t , ψ^t , and their conjugates are related to \mathbf{X}^t , and thus the average over \mathbf{X}^t is taken outside of their integral.

We next take the average over a random graph. In Eq. (17), only the final term in the exponent is relevant to A . We denote this term as \mathcal{L}_2 . We also let $\Xi_{ij}^t = \sum_{\mu} \left(\hat{\psi}_{\sigma_i\sigma_j}^{t,\mu} \phi(x_{j\mu}^t) + \hat{\psi}_{\sigma_j\sigma_i}^{t,\mu} \phi(x_{i\mu}^t) \right) / N$.

Because the graph is generated from the SBM, we have that

$$\langle e^{\mathcal{L}_2} \rangle_A = \prod_{i < j} \left[\sum_{A_{ij} \in \{0,1\}} \left(\rho_{\sigma_i \sigma_j} e^{\Xi_{ij}^t} \right)^{A_{ij}} (1 - \rho_{\sigma_i \sigma_j})^{1-A_{ij}} \right] \quad (18)$$

$$\approx \exp \left[\sum_{i < j} \rho_{\sigma_i \sigma_j} \left(e^{\Xi_{ij}^t} - 1 \right) \right] \quad (19)$$

$$\approx \exp \left[\sum_{i < j} \rho_{\sigma_i \sigma_j} \Xi_{ij}^t \right] \quad (20)$$

$$= \exp \left[\sum_{\mu} \sum_{\sigma \sigma'} \gamma_{\sigma} \rho_{\sigma \sigma'} \hat{\psi}_{\sigma \sigma'}^{t, \mu} \sum_{j \in V_{\sigma'}} \phi(x_{j\mu}^t) \right]. \quad (21)$$

At the second line, we used the fact that $\rho_{\sigma \sigma'} = O(N^{-1})$. Then, at the third line we used $\Xi_{ij}^t = O(D/N) \ll 1$. Finally, at the last line we used the symmetry of the undirected graph, $\rho_{\sigma \sigma'} = \rho_{\sigma' \sigma}$.

Note here that the degrees of freedom with respect to the feature dimension are factored out, and thus the dependence on μ can be omitted. Hereafter, the same notation will be employed for the variables without the μ -dependence. We also introduce the notation $\exp^D(f) \equiv \exp(Df)$. The factor inside of the average over \mathbf{X}^t in Eq. (17) can be written as follows:

$$\begin{aligned} & \int \mathcal{D}\hat{\mathbf{u}}^{t+1} \mathcal{D}\mathbf{u}^{t+1} \int \mathcal{D}\hat{\mathbf{v}}^t \mathcal{D}\mathbf{v}^t \int \mathcal{D}\hat{\psi}^t \mathcal{D}\psi^t e^{\mathcal{L}^*(\hat{\mathbf{u}}^{t+1})} \times \exp^D \left[\sum_{\sigma \sigma'} B_{\sigma \sigma'} \hat{\psi}_{\sigma \sigma'}^t \frac{1}{\gamma_{\sigma'} N} \sum_{j \in V_{\sigma'}} \phi(x_j^t) \right. \\ & \left. + \sum_{\sigma \sigma'} \left(\frac{1}{2} u_{\sigma \sigma'}^{t+1} v_{\sigma \sigma'}^t - \hat{u}_{\sigma \sigma'}^{t+1} u_{\sigma \sigma'}^{t+1} - \hat{v}_{\sigma \sigma'}^t v_{\sigma \sigma'}^t - \hat{\psi}_{\sigma \sigma'}^t \psi_{\sigma \sigma'}^t - \hat{v}_{\sigma \sigma'}^t \sum_{\bar{\sigma} \bar{\sigma}'} \psi_{\sigma \bar{\sigma}}^t \psi_{\sigma' \bar{\sigma}'}^t \right) \right], \end{aligned} \quad (22)$$

where

$$\mathcal{L}^*(\hat{\mathbf{u}}^{t+1}) = \log \int \mathcal{D}\hat{\mathbf{x}}^{t+1} \mathcal{D}\mathbf{x}^{t+1} \exp^D \left(- \sum_{\sigma} \gamma_{\sigma} \hat{x}_{\sigma}^{t+1} x_{\sigma}^{t+1} + \sum_{\sigma \sigma'} \hat{u}_{\sigma \sigma'}^{t+1} \hat{x}_{\sigma}^{t+1} \hat{x}_{\sigma'}^{t+1} \right). \quad (23)$$

As in the main text, we have defined $B_{\sigma \sigma'} \equiv N \gamma_{\sigma} \rho_{\sigma \sigma'} \gamma_{\sigma'}$.

When $D \gg 1$, the saddle-point condition of the exponent in Eq. (22) yields $u_{\sigma \sigma'}^{t+1} = \langle \hat{x}_{\sigma}^{t+1} \hat{x}_{\sigma'}^{t+1} \rangle_{\mathcal{L}^*}$, $v_{\sigma \sigma'}^t = \psi_{\sigma}^t \psi_{\sigma'}^t$, $\psi_{\sigma \sigma'}^t = B_{\sigma \sigma'} (\gamma_{\sigma'} N)^{-1} \sum_{j \in V_{\sigma'}} \phi(x_j^t)$, $\hat{u}_{\sigma \sigma'}^{t+1} = v_{\sigma \sigma'}^t / 2$, $\hat{v}_{\sigma \sigma'}^t = u_{\sigma \sigma'}^{t+1} / 2$, and $\hat{\psi}_{\sigma \sigma'}^t = \sum_{\bar{\sigma}} (\hat{v}_{\sigma \bar{\sigma}}^t + \hat{v}_{\bar{\sigma} \sigma}^t) \psi_{\bar{\sigma}}^t$, where $\psi_{\sigma}^t \equiv \sum_{\bar{\sigma}} \psi_{\sigma \bar{\sigma}}^t$, and $\langle \dots \rangle_{\mathcal{L}^*}$ is the average taken with the weight of the integrand of Eq. (23). Because the correlation between the auxiliary variables should be zero, owing to causality [26, 28], we finally arrive at

$$1 = \int \mathcal{D}\hat{\mathbf{x}}^{t+1} \mathcal{D}\mathbf{x}^{t+1} \exp \left(- \sum_{\sigma} \gamma_{\sigma} \hat{x}_{\sigma}^{t+1} x_{\sigma}^{t+1} \right) \left\langle \exp \left(\frac{1}{2} \sum_{\sigma \sigma'} \hat{x}_{\sigma}^{t+1} F_{\sigma \sigma'}(\mathbf{X}^t) \hat{x}_{\sigma'}^{t+1} \right) \right\rangle_{\mathbf{X}^t}, \quad (24)$$

where $F_{\sigma \sigma'}(\mathbf{X}^t)$ is defined as

$$F_{\sigma \sigma'}(\mathbf{X}^t) \equiv \sum_{\bar{\sigma} \bar{\sigma}'} B_{\sigma \bar{\sigma}} B_{\sigma' \bar{\sigma}'} \frac{1}{\gamma_{\bar{\sigma}} N} \frac{1}{\gamma_{\bar{\sigma}'} N} \sum_{k \in V_{\bar{\sigma}}} \sum_{\ell \in V_{\bar{\sigma}'}} \phi(x_k^t) \phi(x_{\ell}^t). \quad (25)$$

A.2 Stochastic process with a correlated noise

Here, we compare Eq. (24) with a Markovian discrete-time stochastic process $y_{\sigma}^{t+1} = \eta_{\sigma}^t$, in which each element is correlated via a random noise, i.e., $\langle \eta_{\sigma}^t \rangle_{\eta} = 0$, and $\langle \eta_{\sigma}^t \eta_{\sigma'}^t \rangle_{\eta} = C_{\sigma \sigma'}$ for any t . The

corresponding normalization condition reads

$$\begin{aligned}
1 &= \int \prod_{\sigma} dy_{\sigma}^{t+1} \left\langle \prod_{\sigma} \delta(y_{\sigma}^{t+1} - \eta_{\sigma}^t) \right\rangle_{\eta} = \int \prod_{\sigma} \gamma_{\sigma} \frac{d\hat{y}_{\sigma}^{t+1} dy_{\sigma}^{t+1}}{2\pi i} \left\langle e^{-\sum_{\sigma} \gamma_{\sigma} \hat{y}_{\sigma}^{t+1} (y_{\sigma}^{t+1} - \eta_{\sigma}^t)} \right\rangle_{\eta} \\
&= \int \mathcal{D}\hat{\mathbf{y}}^{t+1} \mathcal{D}\mathbf{y}^{t+1} e^{-\sum_{\sigma} \gamma_{\sigma} \hat{y}_{\sigma}^{t+1} y_{\sigma}^{t+1}} \int \prod_{\sigma} \frac{d\eta_{\sigma}^t}{2\pi i} \exp\left(-\frac{1}{2} \sum_{\sigma\sigma'} \eta_{\sigma}^t C_{\sigma\sigma'}^{-1} \eta_{\sigma'}^t + \sum_{\sigma} \gamma_{\sigma} \hat{y}_{\sigma}^{t+1} \eta_{\sigma}^t\right) \\
&= \int \mathcal{D}\hat{\mathbf{y}}^{t+1} \mathcal{D}\mathbf{y}^{t+1} \exp\left(-\sum_{\sigma} \gamma_{\sigma} \hat{y}_{\sigma}^{t+1} y_{\sigma}^{t+1} + \frac{1}{2} \sum_{\sigma\sigma'} \hat{y}_{\sigma}^{t+1} \gamma_{\sigma} C_{\sigma\sigma'} \gamma_{\sigma'} \hat{y}_{\sigma'}^{t+1}\right). \quad (26)
\end{aligned}$$

Analogously to the case of the GNN, we have defined $\mathcal{D}\hat{\mathbf{y}}^{t+1} \mathcal{D}\mathbf{y}^{t+1} \equiv \prod_{\sigma} \gamma_{\sigma} d\hat{y}_{\sigma}^{t+1} dy_{\sigma}^{t+1} / 2\pi i$.

A.3 Self-consistent equation

Finally, we compare Eqs. (24) and (26). However, note that these are not of exactly the same form, because the average over \mathbf{X}^t is taken outside of the exponential in Eq. (24). Two approximations are made in order to derive the self-consistent equation, and the assumptions that justify these approximations are discussed afterward.

First, if the approximation

$$\left\langle \exp\left(\frac{1}{2} \sum_{\sigma\sigma'} \hat{x}_{\sigma}^{t+1} F_{\sigma\sigma'}(\mathbf{X}^t) \hat{x}_{\sigma'}^{t+1}\right) \right\rangle_{\mathbf{X}^t} \approx \exp\left(\frac{1}{2} \sum_{\sigma\sigma'} \hat{x}_{\sigma}^{t+1} \langle F_{\sigma\sigma'}(\mathbf{X}^t) \rangle_{\mathbf{X}^t} \hat{x}_{\sigma'}^{t+1}\right) \quad (27)$$

holds in the stationary limit, then the group-wise state \mathbf{x}^t can be regarded as a Gaussian variable whose correlation matrix obeys

$$C_{\sigma\sigma'} = \frac{1}{\gamma_{\sigma} \gamma_{\sigma'}} \sum_{\sigma_1 \sigma_2} B_{\sigma\sigma_1} B_{\sigma_2\sigma'} \left\langle \frac{1}{\gamma_{\bar{\sigma}} N \gamma_{\bar{\sigma}'} N} \sum_{i \in V_{\bar{\sigma}}} \sum_{j \in V_{\bar{\sigma}'}} \phi(x_i) \phi(x_j) \right\rangle_{\mathbf{X}^t}. \quad (28)$$

This equation is still not closed, because the right-hand side of Eq. (28) depends on the statistic of \mathbf{X}^t , rather than \mathbf{x}^t . However, because the vertices within the group σ are statistically equivalent, $\{x_i\}_{i \in V_{\sigma}}$ are expected to obey the same distribution with mean x_{σ} , which itself is a random variable. If $\sum_{i \in V_{\sigma}} \phi(x_i) / (\gamma_{\sigma} N) \approx \phi(x_{\sigma})$ holds, then the right-hand side of Eq. (28) can be evaluated as the average with respect to the group-wise variable \mathbf{x}^t . Then, within this regime we arrive at the following self-consistent equation with respect to the covariance matrix $\mathbf{C} = [C_{\sigma\sigma'}]$:

$$C_{\sigma\sigma'} = \frac{1}{\gamma_{\sigma} \gamma_{\sigma'}} \sum_{\bar{\sigma}\bar{\sigma}'} B_{\sigma\bar{\sigma}} B_{\bar{\sigma}'\sigma'} \int \frac{d\mathbf{x} e^{-\frac{1}{2} \mathbf{x}^T \mathbf{C}^{-1} \mathbf{x}}}{(2\pi)^{\frac{N}{2}} \sqrt{\det \mathbf{C}}} \phi(x_{\bar{\sigma}}) \phi(x_{\bar{\sigma}'}). \quad (29)$$

Let us consider the first approximation that we adopted in Eq. (27). In the terminology of physics, this is the replacement of a free energy with an internal energy, or the neglect of the entropic contribution. It is difficult to evaluate this residual in general. However, note that this becomes closer to equality as every x_i approaches the same value. Therefore, this implies that the self-consistent equation is more accurate as we approach the detectability limit, and yields an adequate estimate of the critical value.

Let us next consider the second approximation we adopted in Eq. (28). Although the law of large numbers with respect to $\phi(x_i)$ (not x_i) ensures that $\sum_{i \in V_{\sigma}} \phi(x_i) / (\gamma_{\sigma} N)$ has a certain value characterized by the group, this may be different from $\phi(x_{\sigma})$. In fact, the relation between these is in general an inequality (Jensen's inequality) when the activation function ϕ is a convex function. The (exact) equality holds only when $\{x_i\}$ is constant or the function ϕ is linear within the considered domain.

The second approximation can be justified in the following cases. The first case is when the fluctuation of $x_i - x_{\sigma_i}$ is negligible compared to the magnitude of x_{σ} . Note that this is the same assumption as we made in the first approximation. To see this precisely, let us express x_i as $x_i = x_{\sigma} + z_i$ for $i \in V_{\sigma}$. We can formally write the probability distribution $P(\{x_i\})$ of $\{x_i\}$ in a hierarchical fashion as follows:

$$P(\{x_i\}) = \int \prod_{\sigma} dx_{\sigma} \int \prod_i dz_i P_{\sigma}(\{x_{\sigma}\}) P(\{x_i\}) \prod_i \delta(z_i - x_i + x_{\sigma_i}), \quad (30)$$

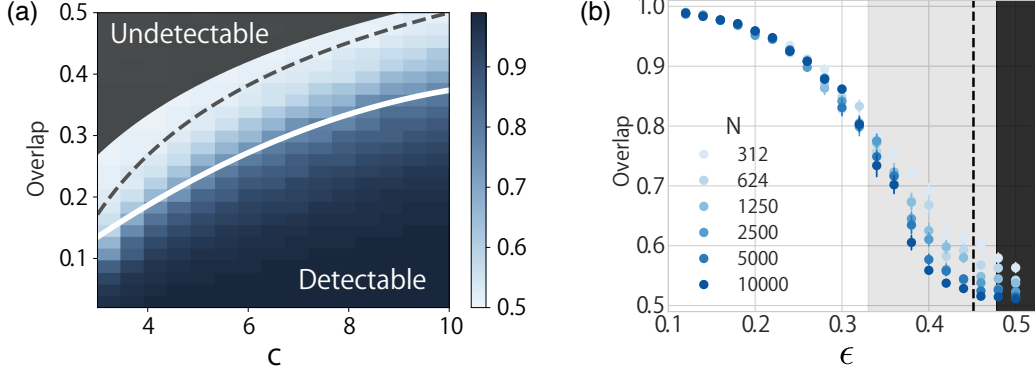


Figure 5: Performance of the untrained GNN using the k-means classifier with $\phi(\mathbf{X})$. (a) The detectability phase diagram and (b) the overlaps of the SBM with $c = 8$ are plotted in the same manner as in Fig. 3 in the main text. When the variation of the overlap is interpolated for each graph size, these curves are crossed at $\epsilon^* \approx 0.33$. It implies the presence of detectability phase transition around the value of ϵ predicted by our mean-field estimate.

where $P_{\sigma}(\{x_{\sigma}\})$ is the probability distribution with respect to \mathbf{x} . Thus, the expectation $\langle f(\mathbf{X}) \rangle_{\mathbf{X}}$ can be expressed as

$$\begin{aligned} \langle f(\mathbf{X}) \rangle_{\mathbf{X}} &\equiv \int \prod_i dx_i P(\{x_i\}) f(\{x_i\}) \\ &= \int \prod_{\sigma} dx_{\sigma} \int \prod_i dz_i P(\{z_i\}|\{x_{\sigma}\}) P_{\sigma}(\{x_{\sigma}\}) f(\{x_{\sigma_i} + z_i\}), \end{aligned} \quad (31)$$

where $P(\{z_i\}|\{x_{\sigma}\}) \equiv P(\{x_{\sigma_i} + z_i\})$, which can be a nontrivial function. However, whenever the contributions from the average with respect to z_i are negligible, Eq. (31) implies that the expectation in Eq. (28) can be evaluated using only the group-wise variables $\{x_{\sigma}\}$. Another case is when the activation function ϕ is almost linear within the domain over which z_i fluctuates. For example, in the case that $\phi = \tanh$, the present approximation does not deteriorate the accuracy even when $x_{\sigma} \approx 0$. When either of these assumption holds, the equality of Jensen's inequality is approximately satisfied, and our derivation of the self-consistent equation is justified.

B K-means classification using $\phi(\mathbf{X})$

Instead of \mathbf{X}^T , $\phi(\mathbf{X}^T)$ can be adopted to perform the k-means classification after the feedforward process. Again, we employ \tanh as the nonlinear activation function. The results of an untrained GNN and a trained GNN under the same experimental settings as in the main text are illustrated in Fig. 5 and Fig. 6, respectively. In Fig. 5a, the reader should note that the range of the color gradient is different from that in the phase diagram in the main text. For the untrained GNN, the obtained overlaps are clearly better than that using \mathbf{X}^T . It can be understood that the error is reduced because the nonlinear function drives each element of the state \mathbf{X}^T to either $+1$ or -1 , making the classification using the k-means method easier and more accurate. On the other hand, for the trained GNN, differences between the overlaps using \mathbf{X}^T and $\phi(\mathbf{X}^T)$ are hardly observable.

Particularly for the case of an untrained GNN in which $\phi(\mathbf{X}^T)$ is adopted for the readout classifier, the overlap gradually changes around the estimated detectability limit. This may be as result of the strong finite-size effect. Again, note that our estimate of the detectability limit is for the case that $N \rightarrow \infty$.

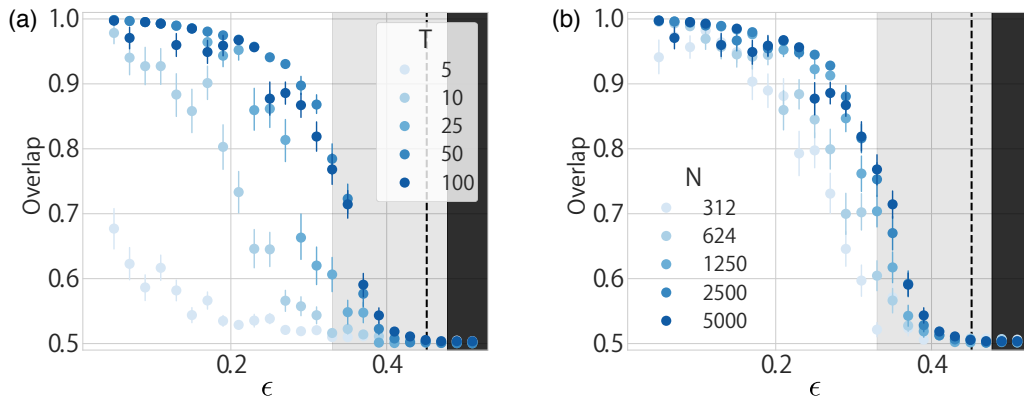


Figure 6: Performance of the trained GNN using the classifier with $\phi(\mathbf{X})$. For (a) and (b), the overlaps are plotted in the same manner as in Fig. 4 in the main text, respectively.